PMSG based Standalone Wind Energy Conversion System with Power Quality Enhancement

Pallavi Chaturvedi *‡, D.K. Palwalia*

*‡, * Department of Electrical Engineering, Rajasthan Technical University, Kota-324010, *INDIA*

(*‡pallavichat9@gmail.com, *dkpalwalia@rtu.ac.in)

Received: 21.02.2023 Accepted:10-.04.2023

Abstract- This paper discusses a novel power quality improvement method for standalone permanent magnet synchronous generator (PMSG) based wind energy conversion system (WECS). The standalone systems are more susceptible to variations in parameters like voltage, frequency, harmonics, etc. These power quality issues can be addressed using an active power filter (APF) integrated at the point of common coupling (PCC). The traditional APF employs Phase-locked loop (PLL), which estimates the angular frequency, and provides limited performance under these variations. The paper proposes a new technique of reference current generation for active power filter (APF) based on the implementation of self-tuning filter (STF). The inclusion of STF instead of conventional low power filter LPF and high-power filter HPF allows direct extraction of the fundamental component in the α-β axis from a distorted electrical signal. This approach achieves simplicity and improved robustness by dispensing with the need for a Phase-locked loop (PLL) in the system. An adaptive hysteresis band current controller (AHBCC) is implemented to generate the switching pattern for regulating the APF by modulating the hysteresis band with system parameters thus maintaining the modulation frequency nearly constant. Mathematical analysis along with MATLAB based simulation results verifies the effectiveness of the proposed topology.

Keywords PMSG, power quality, harmonics, self-tuning filter, adaptive hysteresis band current controller.

1. Introduction

In remote locations, power transmission from the grid is either expensive or non-feasible. In such isolated places standalone renewable energy sources like wind, solar, tidal, biofuels and hydrogen are becoming promising sources of energy. These renewable energy sources can be used for mid and small-scale power generation at an economic and competitive rate as compared to the traditional system [1]. The wind energy conversion system (WECS) meets the criteria for becoming a better alternative for conventional sources [2]. Variable speed wind turbine (WT) is widely used as compare to wind turbine with gearbox [3]. Wind turbine operates at constant speed however these variable speed WT can be operated with generators like induction generator, both squirrel cage (SCIG) and doubly fed induction generator (DFIG) as well as PMSG, which are widely used for low and medium power applications [4]. Gearless speed regulation and high torque at low speed are major advantage of this WT system [5]. The permanent magnet generators offer several advantages over conventional generators. It eliminates need of gears that leads to increase in overall efficiency and system reliability while decreasing total weight of unit and maintenance cost [6]. The standalone wind energy conversion system (SWECS) comprises of power electronics interface converter (AC-DC, DC-DC, DC-AC) between WECS and network [7]. Modern days consumer load including large industries and domestic loads are non-linear in nature and inject harmonic in system owing to large power electronic switching application which may lead to critical issues like equipment failure, resonance, power loss, conductor heating, and delivery system reliability [8]. Passive filters are used to eliminate harmonic distortion as they are simple and economical [9]. However, it has limitations of bulky structure and is designed to compensate for certain set of harmonics. Therefore, due to limitations like fixed compensation, large sizes, limited filtering and specific load range enhanced filter technologies like static synchronous compensator (SSC), dynamic voltage regulator (DVR), active power filter (APF) [10], unified power quality conditioning (UPQC) [11], multilevel inverter [12] were introduced. The shunt active power filters (SAPF) are used at utility side to compensate for current and voltage harmonics, phase balancing, reactive power compensation etc. A SAPF consist of VSI inverter with input inductive coupling and self supported DC capacitor bus.

SAPF's ability to compensate current harmonics relies on precise estimation of reference current [13]. The reference current generation methods have been categorized as time domain and frequency domain [14]. Time domain-based

techniques like instantaneous power(p-q) theory and synchronous reference frame (SRF) (or d-q), remain the preferred methods as they are easier to implement. This reduces controller complexity and, as a result, simplifies the process of practical implementation.

Time domain reference current generation method algorithms are simple as compare to their alternatives in the frequency domain. However, it suffers from possible drawbacks that in turn limits SAPF's capacity [15]. One significant disadvantage of algorithm like the SRF method is the requirement of phase locked loop (PLL) to derive synchronization reference phase. Inclusion of PLL necessitates careful implementation if the source voltages are non-sinusoidal or unbalanced [16]. Although, the p-q theory approach has no requirement for a PLL block, however using this, computing effort of the controller increases due to the additional need for active and reactive power estimation and increased number of voltage transformation steps. In addition to it, for obtaining reference current both p-q and SRF theory algorithms rely on either high pass filter (HPF) or low-pass filter (LPF) to derive their power and current components respectively [17]. As LPF provides better harmonic mitigation performance, it is preferred for reference current generation. However, when fundamental component of current/voltage has high amount of ripples, LPF could not provide precise fundamental reference current/voltage generation.

STF can be incorporated to filter the harmonic present in the sensed voltage and current in order to improve the accuracy and stability of the control system. STF has been integrated with both SRF [18] and p-q theory [19] to work effectively under balanced as well as distorted voltage conditions. The STF when integrated with SRF based algorithm, improves the performance of PLLs under distorted source voltages [20]. In case of p-q theory based (STF-pq) algorithm, STF replaces HPF to generate sinusoidal reference voltage for proper synchronization when the source voltage is non-sinusoidal. STF–pq theory algorithm uses two STFs simultaneously where one STF is used to filter voltage harmonic from distorted source voltage and the other STF filter harmonic component from load current [21]. Together these two filtered voltages and current components are used for estimation of active and reactive power. STF algorithm does not require PLL and is effective in steady-state and dynamic conditions. However, it has increased computational burden and generates non-sinusoidal reference current owing to dependency on fixed gain value. Therefore, due to non-sinusoidal reference current generation by the present pq theory, SRF technique, and STF-pq theory-based algorithms, the direct current control (DCC) scheme is employed to provide the desired switching pulses for regulating the SAPF's mitigation operation [22]. As reported, SAPF switching operation induces switching ripples which in turn pollutes source current and hence degrades the compensating current quality. In the DCC scheme, the switching pulses generated by comparing non-sinusoidal reference current with the measured compensating current (SAPF output current) do not convey precise information of the measured source current. Hence DCC scheme is unable to reduce the problem of source current contamination by switching ripples due to lack of essential information. In this paper, an improved reference current generation scheme is proposed by including a self-tuning (STF) suitable for SAPF's control under distorted voltage conditions. An indirect current control (ICC) scheme is implemented to generate PWM signals by comparing sinusoidal reference source current with actual reference current overcomes this weakness of the DCC scheme. It is devoid of switching ripples problem and therefore provides better harmonic mitigation as it has the precise characteristic of actual source current [23].

This paper presents an improved time domain based current control algorithm that operates under ICC scheme. It employs STF technique for efficient performance even under the condition when source voltage is non-sinusoidal. The proposed scheme generates the required reference current precisely by employing STF technique and therefore ensures that even under non- sinusoidal source voltage condition the SAPF is able to perform effectively by providing synchronization reference phase as well as by generating desired reference current.

Further, the proposed scheme act as the current controller for the power converter. This inner current loop controller generates the suitable switching pattern for the IGBT's of the VSI by using various current control technique such as periodical- sampling controller, triangular current controller, sinusoidal-PWM [24] and hysteresis current controller. Among the different strategies proposed the hysteresis band current controller (HBCC) is preferred due to its simplicity, ease of implementation, fast dynamic response, and robustness towards load perturbations. In conventional HBCC, inverter current is modulated in predefined hysteresis band to achieve low THD. This leads to higher switching frequency which exhibit large variation in switching frequency (uneven switching frequency). At higher value of switching frequency, these large variations in frequency cause significant switching losses, reduced efficiency. It lead to acoustic noise, difficulty in filter design and complex hardware implementation [25]. To overcome these limitations, adaptive-HCC is implemented which offers variable hysteresis bandwidth and reduced in switching frequency variations.

2.System Description

Fig. 1 shows the schematic circuit diagram and control scheme for a WT driven PMSG based wind energy conversion system in an isolated mode.

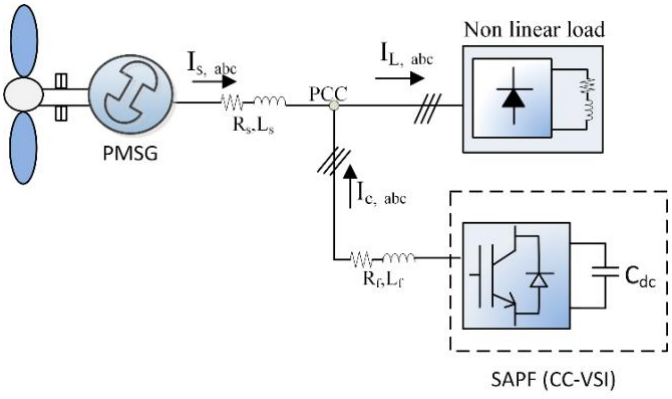

Fig.1 Basic topology of the scheme.

A conventional two-level current controlled voltage source inverter (CC-VSI) with input coupling inductor and DC link capacitor act as the SAPF is connected at the point of common coupling (PCC). The DC bus capacitor and input filter L_f, R_f act as filter that minimizes the switching ripples generated. A three-phase line impedance L_S, R_S feds a diode bridge rectifier with a resistive inductive load used as a non-linear load for simulation.

3.Control Strategies

A typical direct driven PMSG terminals feed the non-linear load as shown in fig.2. Harmonics induced by the power inverter's switching action is suppressed by connecting shunt APF at PCC through filter inductance. The proposed scheme is divided into two sections. The first is a controller for reference current extraction that employs STF and the PI controller to generate unit current vectors. The PI controller regulates the DC capacitor voltage of the CC–VSI. Second, for a PWM-current controlled voltage source inverter, an adaptive HBCC switching control approach is used. The instantaneous load current (I_{La}, I_{Lb}, I_{Lc}) is sensed and is transformed using Clarke's transformation to α-β coordinates which further is **c**onverted to unit current vector templates. The amplitude of these templates is unity in steady-state and may vary under varying load conditions. The sensed voltage of DC-link capacitor voltage V_{dc} and reference voltage $V_{dc,ref}$ are used to measure a voltage error V_e. This error then processed through a proportional integral (PI) controller to estimate the current loss component , which is necessary for controlling the DC-link voltage of VSI.

The desired reference current (I_{sa}*, I_{sb}*, I_{sc}*) is generated by multiplication of the PI controller output and unit vector templates. The reference current is processed through AHBCC to obtain desired switching pulses.

3.1 Hysteresis based current controller

The performance and effectiveness of APF depend on the type of controller and control algorithm used with it. The controller used decides the switching pattern for the CC-VSI of the APF, thereby achieving the desired compensation for current harmonics. Among various methods, HBCC is the preferred method because of its advantages like better stability, good precision, high accuracy, ease of implementation, and simplicity [26]. In HBCC, the resulting error is obtained by comparing the actual current with the reference current. In it, the hysteresis compensator forces the measured current to follow the estimated reference current in a limited fixed predefined range. The hysteresis controller determines the switching signals when subjected to errors obtained by comparing the two current. The lower and upper switches are turned ON when the error surpasses the upper (+HB) and lower (-HB) boundaries of the hysteresis band. This forces the actual current to remain within the hysteresis band as shown in fig.3. The switching frequency of HBCC is determined by the rate at which current changes between the two limits of the tolerance band. Hence, the switching frequency is not stable as the shape of the current wave changes over time. Parameters like line inductance and capacitor voltage determine the rate of change of current. Increase in the switching frequency help to improve the compensating current waveform. However, it can be increased within limits as switching losses and EMI are directly proportional to it as well as there is device switching frequency limitation as well. Therefore, the fixed hysteresis band current control method exhibits disadvantages of uneven switching frequency, makes difficult to design input filters and causes acoustic noise. The proposed AHBCC adjust the hysteresis bandwidth in response to change in instantaneous current and capacitor voltage.

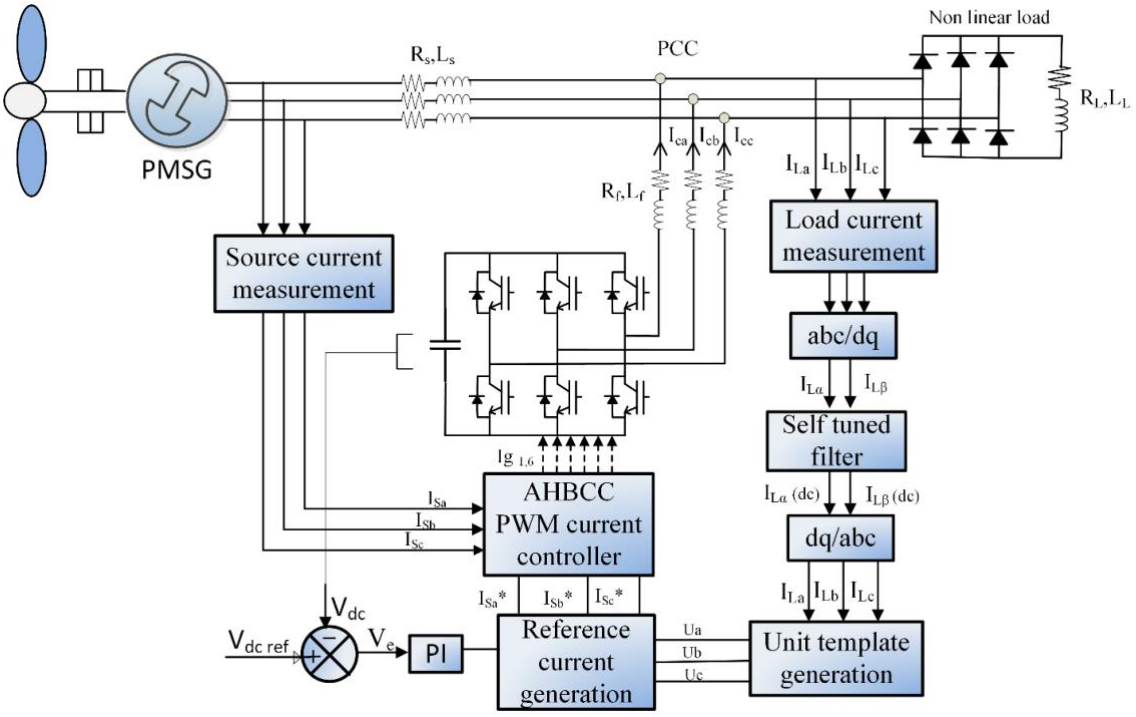

Fig.2. Schematic diagram of STF based active power filter scheme.

The switching pattern of CC-VSI can be controlled by modulating the hysteresis band (HB) at a discrete point of the fundamental frequency cycle. A MATLAB based s-function is designed to generate switching pulses using variable bandwidth.

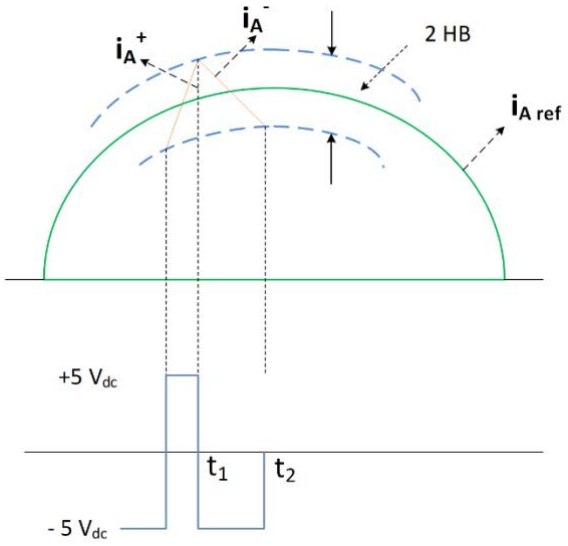

Fig.3. Current waveform with HBCC.

3.2 DC link voltage (V_{dc}) PI controller

The DC-link voltage is regulated by comparing its measured value with the reference voltage. The resulting voltage error is passed through the PI controller. This can be expressed by the following equations:

$$\text{Error} = V_e = V_{dc}^{ref} - V_{dc}^{actual}$$

$$\text{Output of PI controller} = k_p V_e + k_i \int V_e\, dt$$

k_p controls dynamic response whereas k_i determines the settling time for DC voltage [2] [10]. The PI controller output determines the peak value of the reference current I_{max}. The desired reference current to compensate for the harmonic component is generated by multiplying the peak current and the unit current vector.

3.3 Principle of Self-Tuning Filter (STF)

A STF is negative feedback looped sinusoidal signal integrator that is used to extract fundamental components of a positive sequence signal from a distorted input signal [27].

A three-phase distorted load current I_L can be expressed in Fourier series as:

$$\left.\begin{aligned} I_{La}(t) &= I_{La1}\sin(\omega t+\emptyset_1)\,c + \sum_{n=2}^{m} I_{Lan}\sin(n\omega t+\emptyset_n) \\ I_{Lb}(t) &= I_{Lb1}\,sin\left(\omega t+\emptyset_1-\frac{2\pi}{3}\right)+\sum_{n=2}^{m} I_{Lbn}\,sin\left(n\omega t+\emptyset_n-\frac{2\pi}{3}\right) \\ I_{Lc}(t) &= I_{Lc1}\sin\left(\omega t+\emptyset_1+\frac{2\pi}{3}\right)+\sum_{n=2}^{m} I_{Lcn}\sin\left(n\omega t+\emptyset_n+\frac{2\pi}{3}\right) \end{aligned}\right\} \quad (1)$$

Where I_{La1}, I_{Lb1}, I_{Lc1}, n & φ are the amplitude of three phase fundamental load current (I_L), order of harmonic and phase delay respectively. These three-phase measured load current I_{Labc} can be transformed into two phase αβ orthogonal coordinates by using Clark's transformation as follows:

$$\begin{bmatrix} I_{L\alpha} \\ I_{L\beta} \end{bmatrix} = \sqrt{\frac{2}{3}}\begin{bmatrix} 1 & \frac{-1}{2} & \frac{-1}{2} \\ 0 & \frac{\sqrt{3}}{2} & \frac{-\sqrt{3}}{2} \end{bmatrix}\begin{bmatrix} I_{La} \\ I_{Lb} \\ I_{Lc} \end{bmatrix} \quad (2)$$

STF is applied to extract the DC component (fundamental) of the load current ($I_{L\alpha\beta}\ (dc)$) that ensures in-phase operation of the APF with the power system.

The LPF is commonly used for computing the fundamental component of any signal (current/voltage). The primary drawback of conventionally applied LPF is the phase lag that it introduces [28]. Further, it does not completely filter out lower order harmonics. The STF overcome these drawbacks by extracting the positive sequence fundamental component of the distorted signal.

The STF principle is based on the extraction of the DC (fundamental) from the distorted signal. The $\alpha\beta$ axis currents can be divided into fundamental (DC) and oscillatory components.

$$\begin{bmatrix} I_{L\alpha} \\ I_{L\beta} \end{bmatrix} = \begin{bmatrix} I_{L\alpha}\ (dc) + \widetilde{I_{L\alpha}} \\ I_{L\beta}(dc) + \widetilde{I_{L\beta}} \end{bmatrix} \quad (3)$$

Where $I_{L\alpha\beta}(dc)$ & $\widetilde{I_{L\alpha\beta}}$ depicts fundamental (DC) and distorted (AC) components of the load current in $\alpha\beta$ domain respectively.

From Eq.2 $I_{L\alpha}$ is obtained as:

$$I_{L\alpha} = \sqrt{\frac{2}{3}}I_{La}(t) - \frac{1}{\sqrt{6}}I_{Lb}(t) - \frac{1}{\sqrt{6}}I_{Lc} \quad (4)$$

By substituting the values of I_{La}, I_{Lb}, I_{Lc} from Eq (1,2) in Eq.4 gives

$$\sqrt{\frac{2}{3}}\{I_{La1}\sin(\omega t+\emptyset_1)+\sum_{n=2}^{m} I_{Lan}\sin(n\omega t+\emptyset_n)\} - \frac{1}{\sqrt{6}}\left\{I_{Lb1}\sin\left(\omega t+\emptyset_1-\frac{2\pi}{3}\right)+\sum_{n=2}^{m} I_{Lbn}\sin\left(n\omega t+\emptyset_n-\frac{2\pi}{3}\right)\right\} - \frac{1}{\sqrt{6}}\left\{I_{Lc1}\sin\left(\omega t+\emptyset_1+\frac{2\pi}{3}\right)+\sum_{n=2}^{m} I_{Lcn}\sin\left(n\omega t+\emptyset_n+\frac{2\pi}{3}\right)\right\} \quad (5)$$

Simplifying to obtain load current component in α and similarly in β coordinates:

$$I_\alpha(t) = \sqrt{\frac{3}{2}}I_1\sin(\omega t+\emptyset_1)+\sqrt{\frac{3}{2}}\sum_n^{\infty} I_n\sin(n\omega t+\emptyset_n) \quad (6a)$$

$$I_\beta(t) = -\sqrt{\frac{3}{2}}I_1\cos(\omega t+\emptyset_1)-\sqrt{\frac{3}{2}}\sum_n^{\infty} I_n\cos(n\omega t+\emptyset_n) \quad (6b)$$

Where I_{La1}, $I_{L2}$and I_{Lan} are the magnitude of fundamental and harmonic load current components respectively.

Integration of a signal in a synchronous reference frame can be defined as [2] :

$$I_{\alpha\beta s}(t) = e^{j\omega t} \int e^{-j\omega t} I_{\alpha\beta e}(t)dt \quad (7)$$

Where $I_{\alpha\beta e}(t)$ and $I_{\alpha\beta s}(t)$ are the instantaneous signals in the synchronous reference frame and stationary reference frame of ωt respectively before and after integration.

Eq. (7) can be stated by transfer function as follows:

$$H(t) = \frac{I_{\alpha\beta s}(t)}{I_{\alpha\beta e}(t)} = e^{j\omega t} \quad (8)$$

Taking Laplace transformation of Eq. (8) it can be described by following transfer function

$$H(s) = \frac{I_{\alpha\beta s}(s)}{I_{\alpha\beta e}(s)} = \frac{s + j\omega}{s^2 + \omega^2} \quad (9)$$

The stationary component in above transfer function can be obtained by tracking the rotating phase angle (ωt). This can be done by using a PLL with a limitation of introducing the phase delay in the system.

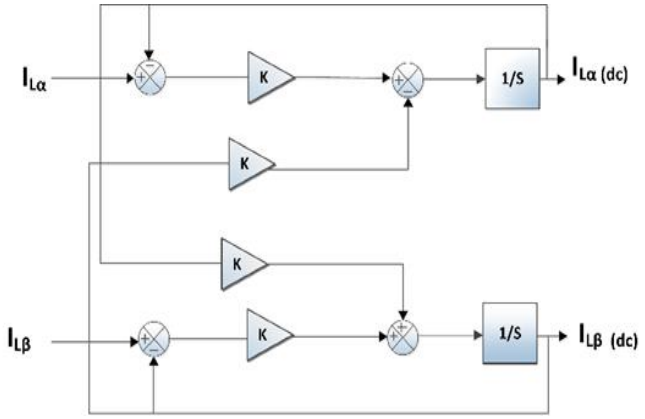

Fig.4. Self tuning filter tuned to fundamental frequency ω_c.

The above problem in transfer function H(s) can be eliminated by addition of constant ***h*** in it. Therefore, the transfer function gets modified as:

$$H(s) = \frac{I_{\alpha\beta s}(s)}{I_{\alpha\beta e}(s)} = h\frac{(s+h) + j\omega}{(s+h)^2 + \omega^2} \quad (10)$$

Fig 4 shows block diagram of STF based control algorithm for determining reference supply current through the extraction of fundamental load current.

Addition of ***h*** limits the magnitude of the transfer function. As the value of ***h*** increases the selectivity of the filter increases simultaneously but at the same time, transient time also increases. Therefore, the gain ***h*** is tuned so that STF extracts fundamental component accurately with reduced time constant and without any phase delay and change in amplitude. At $\omega = \omega_c$ (cut off frequency) the transfer function magnitude equals to 1 and phase delay is equal to zero. 1/***h*** is defined as the time constant of STF.

Simplifying and applying inverse Laplace's Transform with cut off frequency ω_c in eq. (10) gives:

$$I_{L\alpha\beta s}(t) = he^{-ht} e^{jw_c t} I_{L\alpha\beta e}(t) \quad (11)$$

Further replacing $I_{\alpha\beta s}(t)$ by $I_\alpha(t) + jI_\beta(t)$ and the output signal $I_{\alpha\beta e}(t)$ by $\bar{I}_\alpha(t) + j\bar{I}_\beta(t)$ and expanding $e^{jw_c t}$ gives:

$$\bar{I}_{L\alpha}(t) + j\,\bar{I}_{L\beta}(t) = he^{-ht}\cos(\omega_c t) + j\,he^{-ht}sin(\omega_c t)] \times [I_{L\alpha}(t) + jI_{L\beta}(t)] \quad (12)$$

Equating real and imaginary parts on both sides we get:

$$\left.\begin{aligned}\bar{I}_\alpha(t) &= [he^{-ht}\{I_\alpha(t)cos(\omega_c t) - I_\alpha(t)sin(\omega_c t)\}] \\ \bar{I}_\beta(t) &= [he^{-ht}\{I_\alpha(t)sin(\omega_c t) + I_\beta(t)cos(\omega_c t)\}]\end{aligned}\right\} \quad (13)$$

Using Laplace transformation and on further simplification eq. (13) can be written as

$$\left.\begin{aligned}\bar{I}_\alpha(s) &= \frac{h}{s}\{A_\alpha(s) - \bar{A}_\alpha(s)\} - \frac{\omega_c}{s}\bar{I}_\beta(s) \\ \bar{I}_\beta(s) &= \frac{h}{s}\{I_\beta(s) - I_\beta(s)\} - \frac{\omega_c}{s}\bar{I}_\alpha(s)\end{aligned}\right\} \quad (14)$$

Fundamental component can be extracted from distorted signal using eq. (14) without any phase delay and amplitude change. Bode plot of STF for varied values of '***h***' parameter is shown in fig.5.

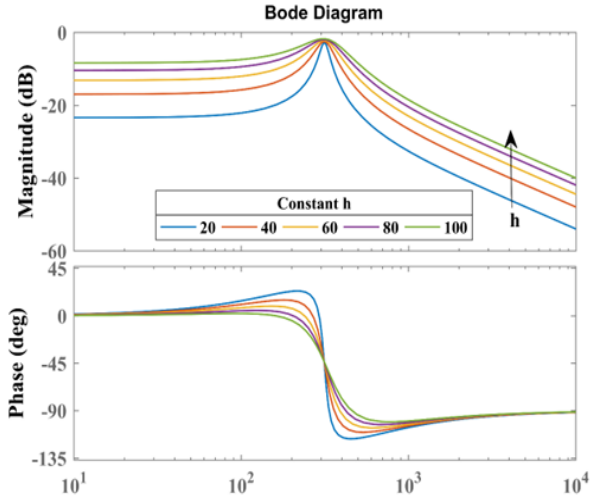

Fig.5. Frequency response plot of STF for varied values of ***h***.

It demonstrates that filter selectivity increases as the value of '***h***' parameter increases. It can also be observed that this filter does not introduce any displacement at fundamental frequency (f_c = 50 Hz). Hence, it can be stated that STF extracts fundamental component from distorted voltage / current signal without change in magnitude or introducing any phase delay.

4. Simulation results and discussion:

A non-linear load is modelled using three phase bridge rectifier (uncontrolled) connected across resistance $R_L = 100\Omega$ and inductor L=100mH.

The STF based compensation control scheme along with adaptive HBCC based switching pattern technique is simulated using MATLAB and results are obtained are discussed. The effectiveness of the scheme is evaluated for various load conditions. Different load conditions chosen are fixed non-linear load, variable non-linear load and unbalanced non-linear load.

Case 1: Fixed non-linear load:

An R-L load across an uncontrolled three-phase rectifier (diode bridge) is connected as non-linear load. Parameters for non-linear load and shunt APF are listed in Appendix.

The simulation results as shown in fig.6 shows the waveform for three phase load current I_{La},I_{Lb} ,I_{Lc} ,load current in αβ axis $I_{L\alpha}$,$I_{L\beta}$, and fundamental current signal extracted for reference current generation $I_{L\alpha(dc)}$,$I_{L\beta(dc)}$ .It can be observed that input to STF $I_{L\alpha}$,$I_{L\beta}$ consist of both harmonic and fundamental component and after STF filtering the output contains only the fundamental current component that validates the efficacy of proposed STF based filtering scheme.

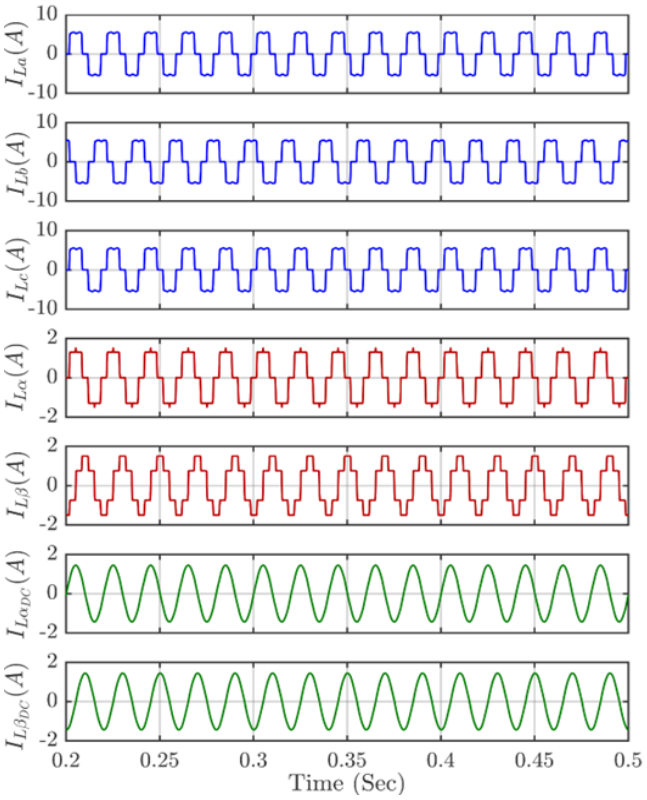

Fig.6. Performance of STF based fundamental current signal extraction under fixed non-linear load condition.

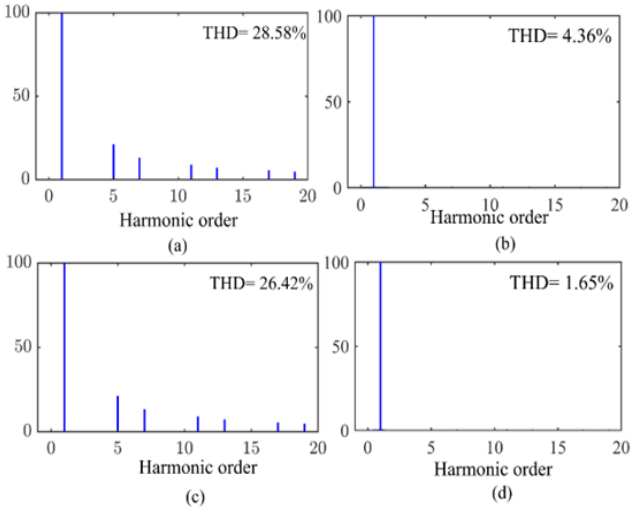

Fig.7. THD values with HBCC of (a) Load current (b)Source current.THD values with AHBCC of (c) Load current (d) Source current.

FFT analysis in fig.7 depicts that THD level of load current and source current for phase 'a' after providing compensation has improved with adaptive hysteresis band current control as compare to fixed band conventional hysteresis band controller from 4.36% to 1.65% which is in compliance with the IEEE 519 standard harmonics distortion limit.

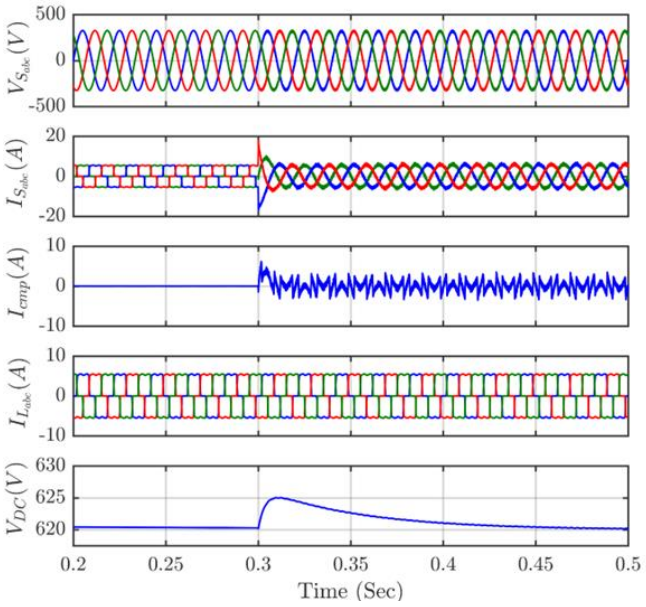

Fig.8. Waveform of generator voltage (V_{sabc}) and current (I_{sabc}), compensating current (I_{cmp}), load current (I_{Labc}), DC bus voltage (V_{DC}) under fixed non-linear load condition.

It is observed from fig.8 that source current becomes sinusoidal after application of SAPF at t= 0.3 seconds.

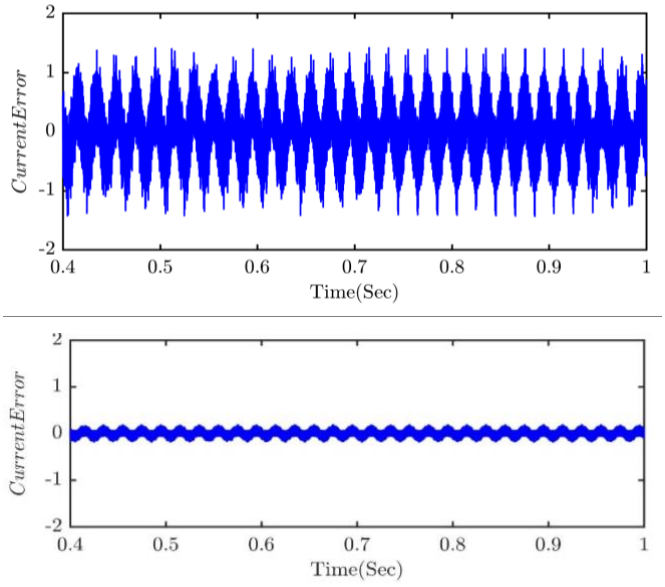

Fig.9.Current error envelope for (a) fixed HBCC (b) AHBCC.

Fig. 9(a) and fig. 9(b) shows the current error envelope ($\delta I_s = I_s^* - I_s$) for fixed HB current controller and adaptive HB current controller. It is seen that the Adaptive HB current controller has small current error envelope as compare to fixed HB current controller. It indicates that tracking error between actual and reference current is minimal in case of AHBCC.

Case 2: Variable non-linear load:

Dynamic performance of STF based proposed control scheme is validated by perturbing the load in step manner.

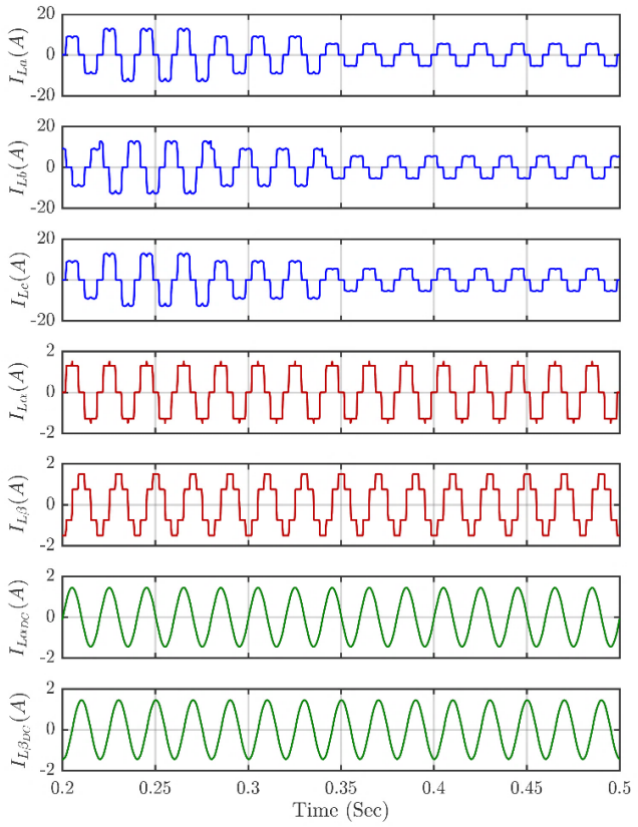

Fig.10. Performance of STF based fundamental current signal extraction under variable non-linear load condition.

Load is first increased at t = 0.24 sec and t = 0.28 sec. It is subsequently disconnected in steps at t = 0.32 sec and t = 0.34 sec.

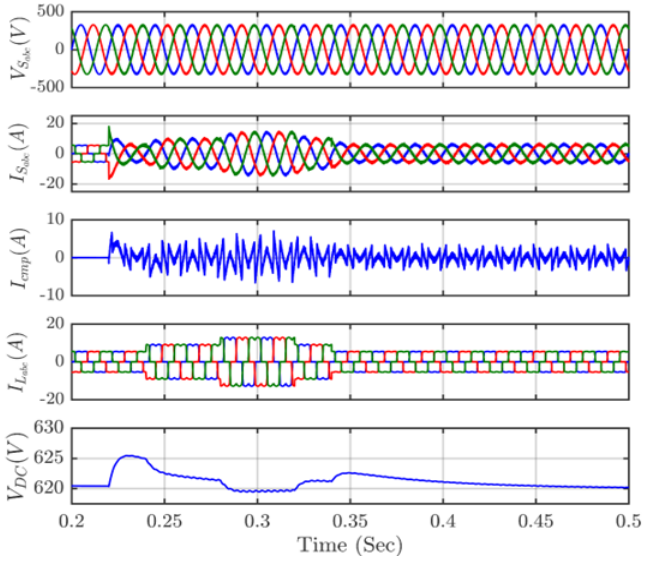

Fig.11. Waveform of generator voltage (Vsabc) and current (Isabc), compensating current (Icmp), load current (ILabc), DC bus voltage (VDC) under variable non-linear load condition.

The simulation shown in fig.10 verifies the performance of STF filter in extracting the fundamental current component even under variable load condition. Simulation results in fig.11 indicates that the controller adequately mitigates the harmonic distortion and fulfill reactive power requirement during the change in load conditions.It is observed that the PI controller effectively regulates the DC-link voltage variation by controlling the peak value of source current.

Case3: Unbalanced non-linear load:

A three phase unbalanced nonlinear load is realized by connecting three single phase rectifiers with unequal resistive and inductive load . Fig.12 shows extraction of fundamental current component by STF filtering during the period of load unbalancing.

Fig.13 shows the waveform of source voltage (V_{Sabc}) with source current (I_{Sabc}), compensating current for phase 'a'(I_{cmp}), load currents (I_{Labc}), voltage across DC link capacitor. The unbalanced load is connected at time t = 0.3 sec resulting in unbalancing in load condition. It is observed that unbalancing in load does not affect the source current that is the generator current and it remains balanced and sinusoidal. This further indicate that inverter controller has isolated the unbalanced load side and the source side. The DC bus voltage (V_{DC}) is also maintained at its reference value during these change in load condition.

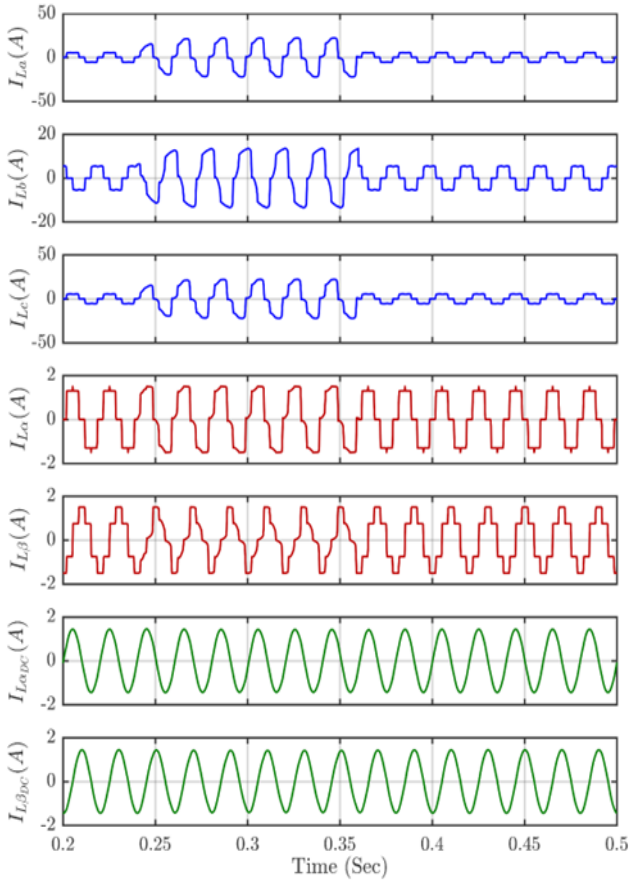

Fig.12. Performance of STF based fundamental current signal extraction under unbalanced non-linear load condition.

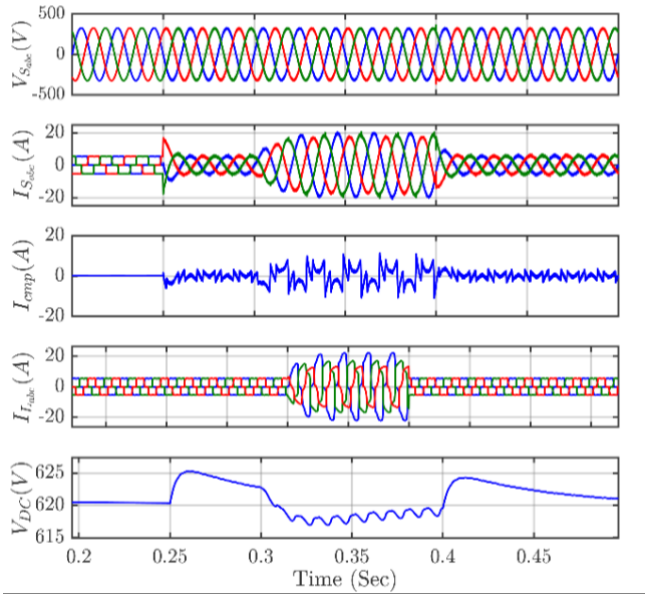

Fig.13. Waveform of generator voltage (V_{sabc}) and current (I_{sabc}), compensating current (I_{cmp}), load current (I_{Labc}), DC bus voltage (V_{DC}) under unbalanced non-linear load condition.

Efficacy of AHBCC over traditional HBCC is validated by improvement in THD level of load as well as source current.

In all three cases discussed, proposed STF based technique is able to filter the harmonic component of load current thus providing only the fundamental component for reference current generation. The PI controller satisfactorily regulates the DC-link voltage variation due to change in load conditions. Efficacy of AHBCC over traditional HBCC is validated by improvement in THD level of load as well as source current.

5. Conclusion

This paper discusses a new STF-based fundamental component extraction algorithm. The harmonics caused by the non-linear load are effectively mitigated by the proposed technique. The sinusoidal reference current is accurately generated by implementing the STF-based algorithm that extracts the fundamental current component from a distorted load current. Performance of the proposed algorithm is analyzed comprehensively for both steady-state and dynamic-state conditions. The proposed algorithm improves the performance without utilizing classical LPF/HPF for harmonic elimination and PLL for phase synchronization. An Adaptive HBCC is used as current controller that provides stable switching frequency. Simulation results suggests that with proposed algorithm low THD levels are achieved in steady state and fast response time during dynamic- state conditions.

Appendix:

PMSG parameters: Power (P) =2.2 KW, no.of poles=5, Armature resistance (R_s)=0.415 ohm, d-axis inductance (L_{sd})=5.13mH, q-axis induactance (L_{sq})=5.13m, Flux linkage(Ψ)=0.121 wb
Load Parameters: Non-linear load :3-phase full bridge diode rectifier with R = 100 ohm, L = 100 mH as load, DC-bus capacitance = 1500 µF, Coupling inductor = 2mH, Constant **h** (STF) = 80.

6. References

[1] Z. Tang, Y. Yang, and F. Blaabjerg, “Power electronics: The enabling technology for renewable energy integration,” CSEE Journal of Power and Energy Systems,vol. 8, no. 1, pp. 39–52, 2022, doi: 10.17775/CSEEJPES.2021.02850.

[2] A. Razmjoo, R. Shirmohammadi, A. Davarpanah, F. Pourfayaz, and A. Aslani, “Stand-alone hybrid energy systems for remote area power generation,” Energy Reports, vol. 5, pp. 231–241, Nov. 2019, doi: 10.1016/J.EGYR.2019.01.010.

[3] R. Tiwari and N. R. Babu, “Recent developments of control strategies for wind energy conversion system,” Renewable and Sustainable Energy Reviews, vol. 66, pp. 268–285, 2016, doi: 10.1016/j.rser.2016.08.005.

[4] A. Chaudhuri, R. Datta, M. P. Kumar, J. P. Davim, and S. Pramanik, “Energy Conversion Strategies for Wind Energy System: Electrical, Mechanical and Material Aspects,” Materials (Basel)., vol. 15, no. 3, pp. 1–34, 2022, doi: 10.3390/ma15031232.

[5] Erdiwansyah, Mahidin, H. Husin, Nasaruddin, M. Zaki, and Muhibbuddin, “A critical review of the integration of renewable energy sources with various technologies,” Protection and Control of Modern Power Systems, vol. 6, no. 1, 2021, doi: 10.1186/s41601-021-00181-3.

[6] E. Hossain, J. Hossain, N. Sakib, and R. Bayindir, “Modelling and Simulation of Permanent Magnet Synchronous Generator Wind Turbine: A Step to Microgrid Technology,” *Int. J. Renew. ENERGY Res.*, vol. 7, no. 1, 2017,doi: 10.20508/ijrer.v7i1.5615.g7013.

[7] S. M. M. Hasan and A. H. M. D. Shatil, “Design and comparison of grid connected permanent magnet synchronous generator non-salient pole and salient pole rotor wind turbine,” AIUB Journal of Science and Engineering, vol. 20, no. 2, pp. 40–46, 2021, doi: 10.53799/AJSE.V20I2.136.

[8] R. B. R. Prakash, P. S. Varma, C. R. Reddy, M. D. Kumar, A. G. Prasad, and E. S. Prasad, “Maximum Power Point Tracking for Permanent Magnet Synchronous Generator based Wind Park Application,” *Int. J. Renew. Energy Res.*, vol. 12, no. 2, pp. 846–862, 2022, doi: 10.20508/ijrer.v12i2.12872.g8469..

[9] L. Motta and N. Faúndes, “Active / passive harmonic filters: Applications, challenges & trends,” Proceedings of International Conference on Harmonics and Quality of Power, ICHQP, vol. 2016-December, no. 1, pp. 657–662, 2016, doi: 10.1109/ICHQP.2016.7783319.

[10] J. Gong, D. Li, T. Wang, W. Pan, and X. Ding, “A comprehensive review of improving power quality using active power filters,” Electric Power Systems Research, vol. 199, no. October 2020, pp. 1073-89, 2021, doi: 10.1016/j.epsr.2021.107389.

[11] E. Jamil, S. Hameed, B. Jamil, and Qurratulain, “Power quality improvement of distribution system with photovoltaic and permanent magnet synchronous generator based renewable energy farm using static synchronous

compensator," Sustainable Energy Technologies and Assessments, vol. 35, no. June, pp. 98–116, 2019, doi: 10.1016/j.seta.2019.06.006.

[12] Jahan, S.; Biswas, S.P.; Hosain, M.K.; Islam, M.R.; Haq, S.; Kouzani, A.Z.; Mahmud, MAP, "An advanced control technique for power quality improvement of grid-tied multilevel inverter," Sustainability (Switzerland), vol. 13, no. 2, pp. 1–20, 2021, doi: 10.3390/su13020505.

[13] Y. Hoon, M. A. M. Radzi, M. A. A. M. Zainuri, and M. A. M. Zawawi, "Shunt active power filter: A review on phase synchronization control techniques," Electronics (Switzerland)., vol. 8, no. 7, pp. 1–20, 2019, doi: 10.3390/electronics8070791.

[14] M. Kashif et al., "A Fast Time-Domain Current Harmonic Extraction Algorithm for Power Quality Improvement Using Three-Phase Active Power Filter," IEEE Access, vol. 8, pp. 103539–103549, 2020, doi: 10.1109/ACCESS.2020.2999088.

[15] O. P. Mahela, B. Khan, H. H. Alhelou, and S. Tanwar, "Assessment of power quality in the utility grid integrated with wind energy generation," IET Power Electronics, vol. 13, no. 13, pp. 2917–2925, 2020, doi: 10.1049/iet-pel.2019.1351.

[16] Y. Hoon, M. A. M. Radzi, M. K. Hassan, and N. F. Mailah, "Operation of Three-Level Inverter-Based Shunt Active Power Filter under Nonideal Grid Voltage Conditions with Dual Fundamental Component Extraction," IEEE Transactions on Power Electronics, vol. 33, no. 9, pp. 7558–7570, 2018, doi: 10.1109/TPEL.2017.2766268.

[17] B. Singh and R. Niwas, "Power quality improvement of PMSG-based DG set feeding three-phase loads," IEEE Transactions on Industry Applications, vol. 52, no. 1, pp. 466–471, 2016, doi: 10.1109/TIA.2015.2480741.

[18] G. Pathak, B. Singh and B. K. Panigrahi, "Permanent Magnet Synchronous Generator Based Wind Energy Conversion System," Eighteenth National Power Systems Conference (NPSC), Guwahati, India, 2014, pp. 1-6, 2014, doi: 10.1109/NPSC.2014.7103862.

[19] Palwalia DK. STATCOM-based voltage and frequency regulator for stand-alone asynchronous generator. International Journal of Power Electronics., vol.6, no.2, pp.131–46, 2014, doi:10.1504/IJPELEC.2014.061469

[20] B. S. Goud and B. L. Rao, "Power quality improvement in hybrid renewable energy source grid-connected system with grey wolf optimization," *Int. J. Renew. Energy Res.*, vol. 10, no. 3, pp. 1264–1276, 2020, doi: 10.20508/ijrer.v10i3.11318.g8004.

[21] Y. Hoon, M. A. M. Radzi, M. K. Hassan, and N. F. Mailah, "A refined self-tuning filter-based instantaneous power theory algorithm for indirect current controlled three-level inverter-based shunt active power filters under non-sinusoidal source voltage conditions," Energies, vol. 10, no. 3, 2017, doi: 10.3390/en10030277.

[22] M. Adel, S. Zaid, and O. Mahgoub, "Improved active power filter performance based on an indirect current control technique," Journal of Power Electronics, vol. 11, no. 6, pp. 931–937, 2011, doi: 10.6113/JPE.2011.11.6.931.

[23] Mahanty R. Indirect current controlled shunt active power filter for power quality improvement. International Journal of Electrical Power and Energy Systems, vol.62, pp. 441–9, 2014, doi: 10.1016/j.ijepes.2014.05.002

[24] S. R. Prusty, S. K. Ram, B. D. Subudhi, and K. K. Mahapatra, "Performance analysis of adaptive band hysteresis current controller for shunt active power filter," International Conference on Emerging Trends in Electrical and Computer Technology, ICETECT 2011, pp. 425–429, 2011, doi: 10.1109/ICETECT.2011.5760154.

[25] K. Poongothai, A. P. F, R. Arunkumar, A. Senthilkumar, and K. Vijayakumar, "An Adaptive Hysteresis Current Control Technique based Shunt Active Power Filter for Power Quality Improvement," International Journal of Engineering Research & Technology (IJERT), vol. 3, no. 16, pp. 1–6, 2015, doi : 10.17577/IJERTCONV3IS16066

[26] M. Kale and E. Ozdemir, "A novel adaptive hysteresis band current controller for shunt active power filter," Electric Power Systems Research, vol. 2, no. July, pp. 1118–1123, 2003, doi: 10.1109/cca.2003.1223167.

[27] A. A. Faiza, S. Morsli, and A. Tayeb, "Self tuning filter based fuzzy logic controller for active power filter," Journal Europeen des Systemes Automatises, vol. 53, no. 5, pp. 739–745, 2020, doi: 10.18280/jesa.530517.

[28] S. Raoul, D. Naoussi, D. S. Haalé, and L. N. Nneme, "STF-pq Approach for Harmonics Mitigation in Stand-Alone PV System," Electrical and Electronic Engineering 2019, vol.9, no.2, pp. 27-34 , 2019, doi: 10.5923/j.eee.20190902.01.